Constraining the Splashback Radius in IllustrisTNG

University of Virginia

Department of Astronomy

Zachary Stevens

Under the guidance of: Dr. Paul Torrey

Submitted in Partial Fulfillment of the Requirements for the

BS Astronomy-Physics Major

Date: May 9, 2024

May 9, 2024
Typeset using LaTeX **twocolumn** style in AASTeX631

Constraining the Splashback Radius in IllustrisTNG

Zachary Stevens,[1] Alex M. Garcia,[1] and Paul Torrey[1]

[1]*Department of Astronomy, University of Virginia, 530 McCormick Road, Charlottesville, VA 22903, USA*

ABSTRACT

Galaxy clusters are the largest structures in the universe and are used as an effective cosmological probe. A common definition of cluster mass is M_{200}, defined as the mass enclosed with within R_{200} – the radius within which the mass density is 200 times greater than the critical density of the universe. However, since R_{200} is not directly observable, M_{200} measurements are challenging to determine. As such, with the upcoming releases of cluster surveys such as Euclid and LSST, constraining cosmological parameters using cluster mass is challenging. The splashback radius, R_{sp}, is a more physically-motivated definition based on infalling material reaching the apocenter of their first orbit. More practically, R_{sp} can also be understood as the radius at which the density profiles of accreting halos is at its steepest. By analyzing cluster properties across the three resolutions of the largest IllustrisTNG simulation (TNG300), we investigate the efficacy of mapping various calculations of R_{sp} to retrieve underlying cluster data. We map relations between 2D and 3D calculations of R_{sp}, along with calculations of R_{sp} using stellar and dark matter particles. In more accurately defining cluster radii observationally, we can more easily define a cluster mass function that can help better constrain cosmological parameters such as σ_8 and Ω_M.

Keywords: evolution - galaxies: cosmology - cosmological constants

1. INTRODUCTION

Galaxy clusters form at the intersection of dark matter (DM) filaments across the universe. Clusters develop as galaxies and dark matter gravitate towards overdense 'nodes' within the cosmic web (White & Rees 1978, Blumenthal et al. 1984). These nodes are understood to have originated from density fluctuations within the early universe that grow due to gravitational amplification. Over cosmic time, these structures grow to become the largest gravitationally bound objects in our universe. The way that these density fluctuations grow throughout cosmic time is determined by cosmological constants σ_8 and Ω_m, which define density fluctuations in the early universe and mass density in the universe (respectively). Critically, we can observe the growth of galaxy clusters throughout cosmic time, providing a deeper understanding of the overall large-structure growth in our universe. As such, the mass of all clusters provide a statistical mass function for our universe that is used a cosmological probe to help derive values of σ_8 and Ω_m (e.g., Bahcall et al., 2003). The way that we currently understand structures throughout the universe is highly dependent on these parameters and our value for them. In cosmological simulations, cluster masses are easily determined; however, in observations, this is more challenging. Currently, the mass contained within galaxy clusters (M_{200}) is defined by the radius at which the density within the cluster drops below 200× the critical density of the universe (R_{200}). In principle, M_{200} can be determined by lensing (Paulin-Henriksson et al. 2007, Radovich et al. 2008), but is difficult to properly evaluate due to a shortage of lensing data. Furthermore, another issue with this definition is that it may not capture all mass accretion across multiple epochs, resulting in an inaccurate interpretation of mass growth at separate times (More et al. 2015).

Ideally, we desire a better definition of galaxy cluster sizes with observational data. Because there are numerous challenges with our current approach for measuring cluster radii, it is difficult to achieve a mass function that accurately develops throughout cosmic time. As such, because determining σ_8 and Ω_m from halo mass functions requires a robust definition of cluster mass,

Corresponding author: Zachary Stevens
zbs2sq@virginia.edu

it is difficult to define these values using observational data. However, if we are able to find a radial definition that is easily observable and accurately represents the total enclosed mass, we will gain a tool that allows us to create the mass function far more easily, and thereafter allow us to more easily calculate σ_8 and Ω_m. Adhikari et al. (2014) propose a new method of defining galaxy clusters using the "splashback radius" (R_{sp}).

R_{sp} is defined as the radius at which mass falling into galaxy clusters reaches the apocenter of its first orbit. Moreover, R_{sp} is a critical method for calculating cluster size because it can be found through evaluation of the density profile, a measurement that can be observed with relative ease. R_{sp} can be derived by finding the steepest gradient in the density profile of the cluster. Because R_{sp} is a quantity that can be determined with relative ease through observations, it is a powerful tool in determining mass functions. R_{sp} is calculated by evaluating the density of the cluster as a function of radius. Then, one finds R_{sp} at the radius where the derivative of the logarithmic density with respect to log radius ($\frac{d(\log(\rho))}{d(\log(r))}$) is at a minimum, often referred to as the first caustic. This minimum should be able to be calculated with observational data, making it a strong candidate for a definition of cluster size.

Because our observations consist solely of stellar light, one should seek a relation between the stellar light and the underlying DM halo within the cluster. Montes & Trujillo (2018) find that intracluster light (ICL) tracks the host DM halo to a high order. The ICL comes from stellar light that is not bound to any of the galaxies within the cluster, and forms from the interactions that occur between galaxies during the formation of the cluster that strip stars from their host galaxies, as described in Gregg & West (1998) and Rudick et al. (2006). Therefore, R_{sp} is calculable using ICL both as an independent radial measurement and to track the host DM halo in which a cluster sits, which provides a second radial measurement.

Our goal with this project is to understand how R_{sp} calculated using our observational data of a cluster can map to the true underlying data of the cluster. Our observational data consists solely of two-dimensional (2D) projections of stellar light within clusters. However, clusters are three-dimensional (3D) objects that are assumed to be roughly spherical, and contain both stellar mass and dark matter. Therefore, we seek a method that allows us to translate our 2D stellar observation of clusters to a more holistic understanding of the 3D data both with stellar light and dark matter.

Therefore, we analyze the efficacy of R_{sp} in mapping clusters across various different calculation methods using the IllustrisTNG simulation. We provide a set of relationships between different calculations of R_{sp} in order to understand how the different variables in calculation relate to each other. First, we compare calculations made with stellar particles and dark matter particles. We then compare R_{sp} calculations done in 2D and 3D. Finally, we investigate how our calculations of R_{sp} change as a function of simulation resolution. These three variables - particle type, dimensionality, and resolution - are critical to understand, as observational data only provides 2D stellar data. Once we understand the relationship between the calculation of R_{sp} with each of these variables, we can provide a mapping for observational data that will give a holistic understanding of cluster mass. In Section 2, we introduce the IllustrisTNG simulation along with describing our different approaches in calculating R_{sp}. In Section 3, we describe how limiting error on our calculated values of R_{sp} affect the correlation between different types of calculations. In Section 4, we proceed to derive a more explicit relationship between each method of computing R_{sp}, and analyze how the constraint of our error changes the derived relationship. We also discuss future steps for the project. We finally summarize our results in Section 5.

2. METHODS

2.1. *The IllustrisTNG Simulations*

For our work, we use the IllustrisTNG (TNG) simulation dataset (Marinacci et al. 2018; Naiman et al. 2018; Nelson et al. 2017; Pillepich et al. 2017; Springel et al. 2017). The TNG project simulates cosmological structures in the universe at numerous resolutions and box sizes, and is 'the next generation' of the original Illustris simulation (Vogelsberger et al. 2014; Genel et al. 2014; Sijacki et al. 2015). TNG consists of three different datasets at three different box sizes of approximately ∼50Mpc, ∼100Mpc, and ∼300Mpc in side length, respectively known as TNG50, TNG100, and TNG300. TNG evolves cosmological structures from the early universe at $z = 127$ using baryonic and dark matter particles. The TNG simulation models many of the processes we see observationally in the universe, taking into account physical processes such as the seeding and growth of supermassive black holes along with their feedback. TNG accurately models the cooling of gas and its magneto-hydrodynamical interactions. These processes give us an accurate understanding of galaxy formation throughout cosmic time. More of the processes that are modeled can be found in Weinberger et al. (2016) and Pillepich et al. (2017). Our dataset uses the TNG300 catalog of the IllustrisTNG simulation with a volume of $(302.6\ \mathrm{Mpc})^3$. It is important to note that while the

other simulations in IllustrisTNG - TNG50 and TNG100 - are higher resolution simulations, the smaller volumes would prohibitively limit our calculations as we are seeking a statistical sample of galaxies that is best provided by the TNG300 simulation. We test the impact of resolution on our results by comparing across the three resolutions TNG300-1, TNG300-2, and TNG300-3. The resolution describes the particle mass and number of particles that are used to simulate the physics within the simulation. The lowest resolution, TNG300-3, uses $(625)^3$ DM and stellar particles. TNG300-2, then, uses $(1250)^3$ particles, and TNG300-1 uses $(2500)^3$. Each simulation increases resolution by a factor of 8, so there is a factor of 64× difference in resolution between TNG300-3 and TNG300-1. As such, we are able to investigate the impact of simulation resolution on our results. A higher number of particles models the hydrodynamical physics at a slightly more accurate level, and so we expect to see slightly different results for each resolution.

The IllustrisTNG simulations use a cosmology defined by the Planck Collaboration XIII (Ade et al. (2016)). These parameters are defined to be $\Omega_m = 0.3089$, $\Omega_b = 0.0486$, $\Omega_\Lambda = 0.6911$, and $h = 0.6774$.

2.2. *Splashback Radius Calculation*

A primary goal of this work is to create a mapping between two-dimensional and three-dimensional calculations of R_{sp}, allowing us to map our observational data to the true underlying data. This informs the way that we choose to calculate the splashback radius. To calculate the splashback radius we first compute the density profile of the halos.

Let us consider a simplistic method of density calculation. One can use a set of spherical shells with volume $\frac{4}{3}\pi dr^3$ and choose a thickness $dr = (R_{outer} - R_{inner})$ for each. Within each of these shells, one can easily calculate density by mass/volume, but this is subject to our choice of dr. By increasing dr, one gets a more accurate measure of density, but the density profile becomes less smooth. If dr is decreased, we return a smoother density function, but one that is more subject to random fluctuations in which particles are or are not within each shell. As such, we want a different method that minimizes the impact of our choice of dr and gives us a smoother density profile.

We choose to use the smoothed-particle hydrodynamics method (SPH) from Monaghan & Lattanzio (1985). We calculate the density profile of our halos using spherical shells along a Fibonacci sphere. We measure the density at numerous points equally distributed over 100 shells between $[0.1 - 4]R_{200}$ using the SPH method. The SPH method is a method of calculating density that uses a kernel function to give a higher weight to particles nearest the chosen point. The radius of this kernel function is chosen to be the radius that encapsulates the 32 nearest particles. We then calculate the density ρ_i at each of the points i on the Fibonacci sphere using

$$\rho_i = \sum_j^{32} m_j W_{ij} \tag{1}$$

from Monaghan & Lattanzio (1985). Within this equation, W_{ij} is a kernel chosen to be a cubic B-spline given by

$$W_{ij} = W(|r_i - r_j|) \tag{2}$$

as a function of the particles' distances $r_{i,j}$ from each other. Mass m_j is given by

$$m_j = \rho_j V_j \tag{3}$$

for particle density ρ_j and particle volume V_j. The methods of the cubic B-spline can be found in more detail in Monaghan & Lattanzio (1985). This method allows us to get a more accurate understanding of the density at each point and produces a smooth density function. For the 2D cylindrical calculation, we choose an arbitrary angle of perspective and perform the same calculation at points along a Fibonacci cylinder. It is important to note that this Fibonacci cylinder is very thin, representing a small slice through the center of the cluster. The cylinder has a radius of $4 \times R_{200}$ and a length of 8kpc, measuring ±4kpc from the center of the cluster. We again calculate density at numerous points along radial shells within the cylinder using the SPH method.

Once our density profile is constructed, we create a plot of the particle density ρ as a function of $\log(r/r_{200})$, and evaluate where $\frac{d\log(\rho)}{d\log(r)}$ is at a minimum. These evaluations are shown in Figure 1, best seen in the blue dotted line in Fig 1a. Often this is a well defined minimum, or caustic, with minimal error bounds.

We seek to provide error on our calculations of R_{sp} at multiple different levels in order to better understand how relationships between methods of R_{sp} calculation change as a function of error. Our method of error calculation is shown in Figure 1. On the left is the density profile of three clusters in the TNG simulation. The right panels show the derivative of the logarithmic density with respect to log radius, in dashed blue. The minimum, where R_{sp} is determined, is shown as a red dot. The red, yellow, and green plots are copies of the original data (blue) that help us calculate the error in our calculation of R_{sp}. We calculate error by first raising the blue plot so that the y-value of R_{sp} is at zero.

Then, we lower the plot by one integer value of $\frac{d\log(\rho)}{d\log(r)}$, shown by the red dashed line. We do this two more times, shown in yellow and green. For each subsequent time that we lower the plot, we calculate the intercept of the corresponding graph with $\frac{dlog(\rho)}{dlog(r)} = 0$, shown as vertical lines that represent the corresponding error. These provide a reasonable estimate of error at three integer steps of $\frac{d\log(\rho)}{d\log(r)}$.

We do this to understand how quickly the error grows as a function of stepping away from R_{sp}. When the error grows quickly between each step size, we understand that R_{sp} is not as well defined. In Figure 1a, we see that all three error steps are constrained to one caustic and do not grow rapidly, representing a well defined splashback radius. In Figure 1b, we see that the red plot (the first step of error) is well constrained to the caustic in which R_{sp} is defined. However, the second integer step (yellow) is far from the first and introduces a secondary caustic into our calculation, while the third step (green) extends even further. This provides a reasonable understanding of how well R_{sp} is being calculated for each halo - it is unreasonable to believe that the single minima is always the correct one, especially if we have secondary caustics. Finally, if none of the steps of error are close to R_{sp}, it is likely that we have a wide minimum as shown in Figure 1c, and should not take R_{sp} to be well defined. Therefore, we should be more hesitant to analyze clusters with high error on their calculations of R_{sp}.

The set of three error values allows us to understand which halos have the best defined values of R_{sp}. If all three error steps are within a small radius of R_{sp}, we understand that we have a halo like in Figure 1a, with a well defined minimum that can be trusted to be an accurate representation of the cluster size. If only the first step of error is within a small radius of R_{sp}, like in Figures 1b, then we may have multiple caustics. If none of the error steps are within a reasonable radius of R_{sp}, then it is likely we have a poorly defined minimum as in Figure 1c.

2.3. *Assembly of Catalogs*

We produce a set of catalogs with the values of R_{sp} and associated error, allowing us to later categorize our halos by their error and derive a subsection of our sample that represents the ideal selection if the splashback radius is calculated perfectly.

The first parameter that we investigate is the impact of resolution. The highest resolution of TNG300, TNG300-1, uses 64x more elements to create its data than the lowest resolution. Therefore, it is important to understand how changing resolution affects our calcula-

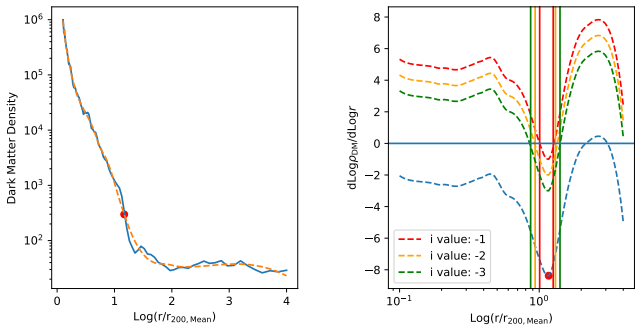

(a) R_{sp} calculated with a well defined minimum.

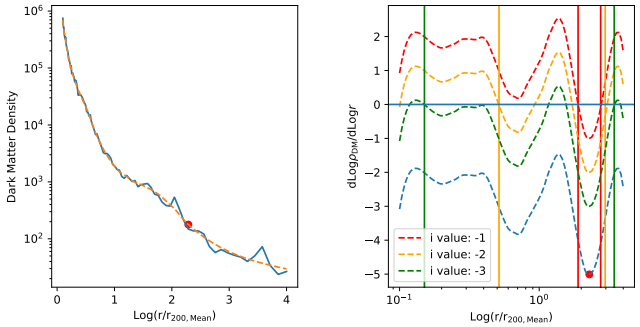

(b) R_{sp} calculated with multiple caustics.

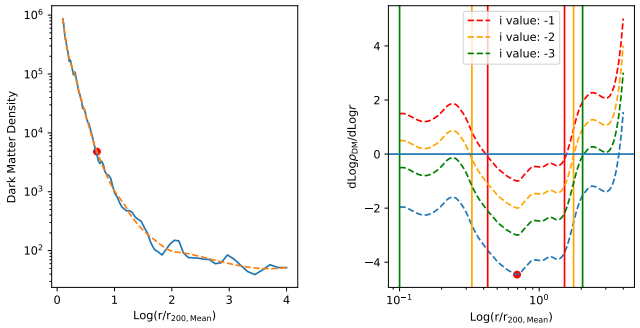

(c) R_{sp} with a poorly defined minimum.

Figure 1: The density profile calculated for three different clusters in the TNG simulation. On the left of each figure is density as a function of r/r_{200}. On the right is the derivative of the density profile as a function of r/r_{200}, shown in blue. The minimum is shown with a red point on the blue plot, defining R_{sp}. The red, yellow, and green plots first raise the blue plot so that the y-value of R_{sp} is at $\frac{d(\log(\rho))}{d(\log(r))} = 0$, then are lowered down in three integer steps to provide error at three values of $\frac{d(\log(\rho))}{d(\log(r))}$. The vertical lines show the corresponding error bars at each step. Panels (a), (b), and (c) depict a well defined value of R_{sp}, a cluster with multiple caustics, and a cluster with a poorly defined minimum, respectively.

tion of R_{sp}, and thus we perform our analyses at each level of resolution in TNG300 and compare across them.

Beyond resolution, we also compare our calculations of R_{sp} using dark matter and stellar particles. It is understood that the ICL, found from stellar light from stars not bound to individual galaxies, effectively traces the underlying DM halos of clusters (Montes & Trujillo 2018). We can first verify the efficacy of this by mapping the measurement of $R_{sp,\mathrm{DM}}$ to $R_{sp,\mathrm{stars}}$. In theory, this should be a near 1:1 relationship because of the relationship between the ICL from stars and the DM halo. Therefore, is important to understand the relationship between DM and stellar particles, and thus we create these separate catalogs so that we can find the correlation between the two.

Finally, we compare catalogs between calculations in 2D and 3D, as discussed above. Comparing the two is critical for understanding how R_{sp} maps between observational data and true 3D data. Our 2D data reflects physical cluster observations, as we only get a projection of the total underlying data by observation. Therefore, we hope to better understand how a calculation of the cluster in 2D may compare to a calculation in 3D to validate whether the splashback radius accurately maps the cluster.

With these three variables in mind - resolution, particle type, and dimensionality - we produce 12 catalogs of R_{sp} calculations with which to perform a statistical analysis. We have 4 catalogs created at each resolution TNG300-1, TNG300-2, and TNG300-3. Within each of these resolutions, there are two 2D and two 3D catalogs. Each of these then contains two catalogs: one calculated with stellar particles and one calculated using DM particles.

3. RESULTS

3.1. *Seeking the Golden Sample*

We first want to determine what our ideal sample of R_{sp} is. As described in Section 2, we have a set of errors corresponding to three integer steps along $\frac{d(\log(\rho))}{d(\log(r))}$ for R_{sp}. Many of our halos have a low set of errors that are narrowly bound around the value of R_{sp}, such as in Figure 1a. Ideally, all three error bars are close together and near the value of R_{sp}, representing a well defined cluster.

We find that for many of our plots comparing calculations of R_{sp}, there is considerable spread around the line of best fit. We consider that this spread may come from outliers that lack a well defined value for R_{sp}. Weighting data points with high error error equally to data points that are well defined could result in points far from our line of best fit widely skewing our results and giving us an inaccurate relationship between the various ways of calculating R_{sp}. Thus, we seek to establish a set of data points with well defined values of R_{sp} such that we can better understand whether our data is being skewed by the effects of poorly calculated radii. This method also provides a way for us to understand how error in our observations affects the relationship between our 2D stellar results and the implied 3D and DM data.

We find that error comes from multiple sources. First, there are often secondary caustics found at different locations within our density profiles, which can appear for numerous reasons and are discussed in more detail in Deason et al. (2020). They note that these secondary caustics often appear at smaller radii and are more common amongst halos that have a lower accretion rate. While understanding these secondary caustics is still a future project, they nevertheless introduce a source of error into our calculation of R_{sp}. Another source of error in the calculation of R_{sp} occurs when the minimum in the graph of $\frac{d\log(\rho)}{d\log(r)}$ is not as well defined, introducing greater uncertainty. We find numerous halos with $\geq$2 caustics and a poorly defined minimum.

Our error is calculated as described above in Section 2.2, resulting in a set of error bars at three steps along $\frac{d(\log(\rho))}{d(\log(r))}$. We now seek to define a so called "Golden Sample" of results that represent the idealized values of R_{sp}.

3.2. *R_{sp} Mapping - Variable Comparison*

We seek an idealized set of halos with low error that return a high correlation in our results, as this represents halos with the most well defined values of R_{sp}. This is accomplished by steadily varying the threshold of how large our error can be and seeing how this affects the derived slope of relation between calculations of R_{sp}. Evaluating the relationship is best understood using the Pearson correlation coefficient, which is plotted across the range of the value of the error threshold, as shown in Figure 2. We create these plots for the three different resolutions of TNG300, and compare between stars and dark matter calculations, along with across 2D and 3D calculations.

In Figure 2a, we find an increasing correlation as a function of resolution, and find reasonable evidence to constrain our data when comparing stellar and DM splashback radii in 3D. In Figure 2b, we find a weak correlation between our stellar and DM splashback radii in 2D, and lack any evidence suggesting that constraining error increases correlation. This is a curious result, and suggests that we may need a new method of approach in how we are calculating our 2D splashback radii.

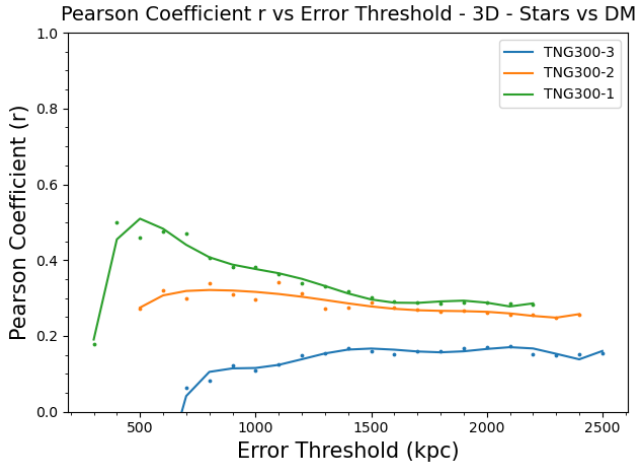

(a) R_{sp} calculated in 3D, comparing stellar to DM calculation.

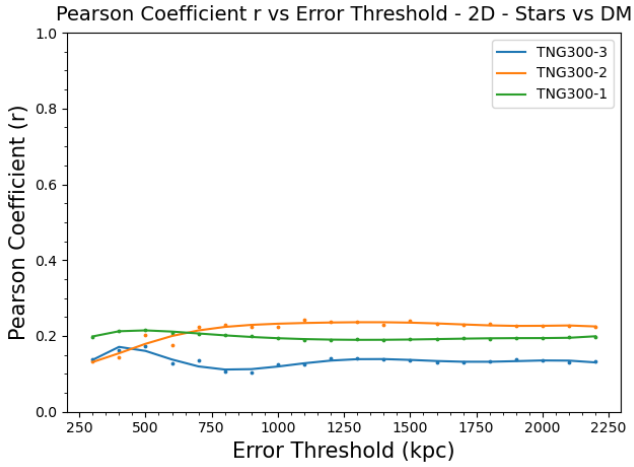

(b) R_{sp} calculated in 2D, comparing stellar to DM calculation.

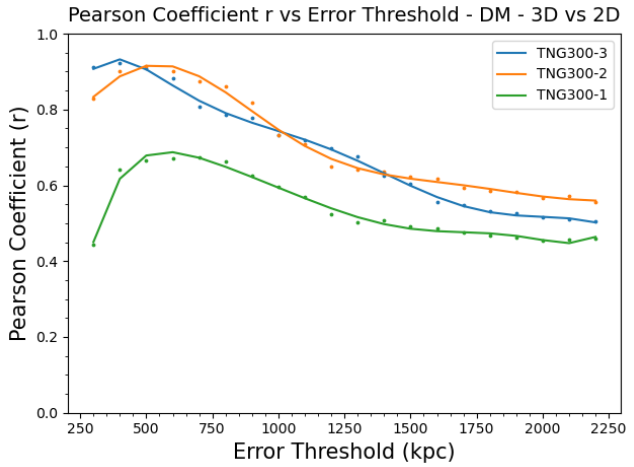

(c) Comparison of R_{sp} calculated using DM particles in 3D and 2D.

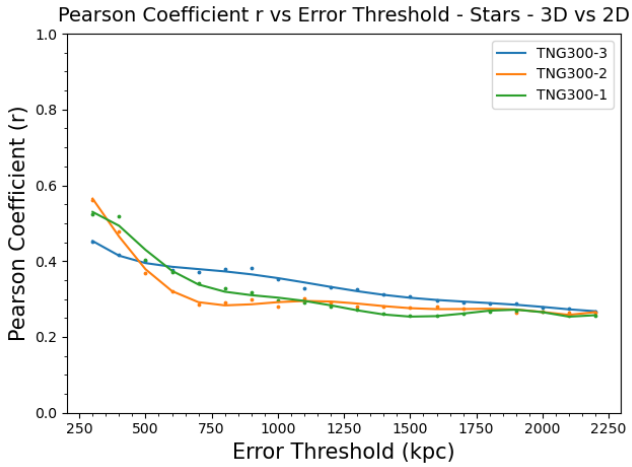

(d) Comparison of R_{sp} calculated using stellar particles in 3D and 2D.

Figure 2: Pearson correlation coefficient r as a function of the error threshold on R_{sp}. Blue represents the lowest resolution, TNG300-3, orange shows the middle resolution (TNG300-2), and green shows the highest resolution, TNG300-1. Each plot show the correlation between two calculations of R_{sp} (noted in the respective captions) as the threshold for error is changed.

In Figure 2c, we find high correlation between our calculations of R_{sp} using dark matter in 2D and 3D. The high correlation is promising, as we should expect a 2D cross section of a spherical structure to return the same radius as a 3D analysis of the same structure. We also find that correlation increases as a function of decreasing our error threshold. This relationship is also promising, as we have already suggested that error on our results may decrease as a function of higher simulation resolution. Therefore, lower error from higher resolution simulations should return a better correlation from 2D to 3D data, suggesting that we can model R_{sp} using DM fairly well purely with 2D data. In Figure 2d, we find a slightly lower correlation between our calculations in 2D and 3D for stellar splashback. We find a similar result to DM in that the correlation increases as our error threshold decreases. However, the lower correlation in our stellar data suggests that there is a difference between DM and stellar calculations of R_{sp}, which should be investigated.

For each pair of R_{sp} results shown in Figure 2, we provide a corresponding graph of the two variables plotted against each other, as in Figures 3 - 6. In each comparison, we show the two variables with a range of error thresholds, increasing in 200 kpc increments. This allows us once again to validate whether our Golden Sample is of any use in narrowing our calculations down to

retrieve a higher correlation or more concrete relationship.

In Figures 3 - 6, we depict $\log(R_{sp})$ vs $\log(R_{sp})$ for each calculation method, and plot both a 1:1 line (red) and a line of best fit (blue), with the correlation coefficient r shown below the line equation in the caption.

We delve deeper into each of these plots below.

4. DISCUSSION

4.1. *Analysis of Error Constraint*

In the following section we observe the various comparisons of correlation between different calculations of R_{sp} in Figure 2, and follow them up in more detail by plotting these calculations against each other. In plotting the various calculations of R_{sp}, we are able to better visualize the relationship between the variables, and discover results that impact our correlation between the calculations. For each set of variables, we discuss the correlation as a function of the imposed error threshold, and follow it up with a set of plots investigating relationships with different error constraints.

4.1.1. *Stars vs DM in 3D*

First, we observe our correlation as a function of our error threshold in Figure 2a. Here, we compare $R_{sp,\mathrm{stars}}$ and $R_{sp,\mathrm{DM}}$ in 3D across the three resolutions of TNG300, and find a significant dependence on resolution.

At the lowest resolution (TNG300-3), the Pearson correlation coefficient does not rise above $r = 0.2$, indicating a poor correlation between $R_{sp,\mathrm{stars}}$ and $R_{sp,\mathrm{DM}}$ for TNG 300-3. There is no value of our error threshold for which we retrieve a significantly higher correlation between our data points - in fact, at lower thresholds, we seem to retrieve a lower correlation. This signifies that at TNG300-3, we do not have a viable 'Golden Sample,' and further that there is no significant reason to make cuts based on error when analyzing data at this resolution.

For TNG300-2, we find that our correlation increases by a factor of approximately 2, but remains a mostly flat result. The comparison at this resolution still only results in a correlation coefficient $r \approx 0.3$ at the peak of this relation. As a result, for TNG300-2, we draw the same conclusions as for TNG300-3; there is no 'Golden Sample.'

For TNG300-1, however, we begin to find a marked increase in correlation between between $R_{sp,\mathrm{stars}}$ and $R_{sp,\mathrm{DM}}$. As we decrease our error threshold, we reach $r \approx 0.5$ at a peak around 500kpc. The peak at an error constraint of 500kpc implies that this is where we will see the highest correlation between stellar and DM R_{sp} calculations in 3D, and that this is where our best data could come from. It also indicates a more significant relation between the two - almost 2× more than for TNG300-2. We also find a notable decrease in correlation as we increase our threshold - far more than for TNG300-3 or TNG300-2 - indicating that creating a 'Golden Sample' for TNG300-1 will create higher correlations between our variables in comparing R_{sp}.

It is important to note the range of the x-axis in these plots as well. We find that as resolution increases, we are able to decrease our error threshold further before the correlation drops off. This is significant as it suggests that at higher resolution we are able to better define R_{sp}. This suggests that in a higher resolution simulation, we could model R_{sp} to a much higher level, with low error on more of our calculations. This would also enable us to find stronger correlations between our data, as suggested by Figure 2.

We can further investigate the impacts of this result on our comparison of R_{sp} calculation by investigating plots of $R^{3D}_{sp,\mathrm{stars}}$ versus $R^{3D}_{sp,\mathrm{DM}}$ with varying the error threshold and comparing these plots to the literature. Deason et al. (2020) find a near 1:1 relationship between the stellar and DM values of R_{sp} with low scatter on the values. Their results are calculated from the data within the C-EAGLE simulation project (Barnes et al. 2017), which has a resolution of ∼1 kpc in space and $1.8 \times 10^6 M_\odot$ and $9.7 \times 10^6 M_\odot$ in mass for baryons and DM, respectively. The highest resolution of TNG 300, TNG300-1, has a resolution of $(302.6)^3$ kpc in space and $1.1 \times 10^7 M_\odot$ and $5.9 \times 10^7 M_\odot$ in mass for baryons and DM, respectively. The larger particles in TNG300 do not allow us to resolve the physics within the simulation as well. Therefore, while TNG300 is a powerful tool for large data analysis, it is unable to create as well resolved values of R_{sp} due to its lower resolution. Therefore we expect more poorly defined values of R_{sp}, leading to the larger spread along the 1:1 fit line.

We find that in changing resolution, correlation between $R^{3D}_{sp,\mathrm{stars}}$ and $R^{3D}_{sp,\mathrm{DM}}$ increases to its greatest value when we use TNG300-1, as demonstrated in Figure 2a. With the TNG300-1 data, we also find that at the error thresholds where the Pearson coefficient r is the highest, the relationship between $R^{3D}_{sp,\mathrm{stars}}$ and $R^{3D}_{sp,\mathrm{DM}}$ is very near a 1:1 relationship, demonstrating a confirmation of the literature.

We proceed by plotting $R^{3D}_{sp,\mathrm{stars}}$ and $R^{3D}_{sp,\mathrm{DM}}$ in Figure 3. In the full dataset, shown on the left, we see the low correlation with a value of $r = 0.26$, and the results only return a slope of 0.46. However, when we restrain our error, we find that our slope converges to be much closer to 1, as we expect (shown in the second panel of

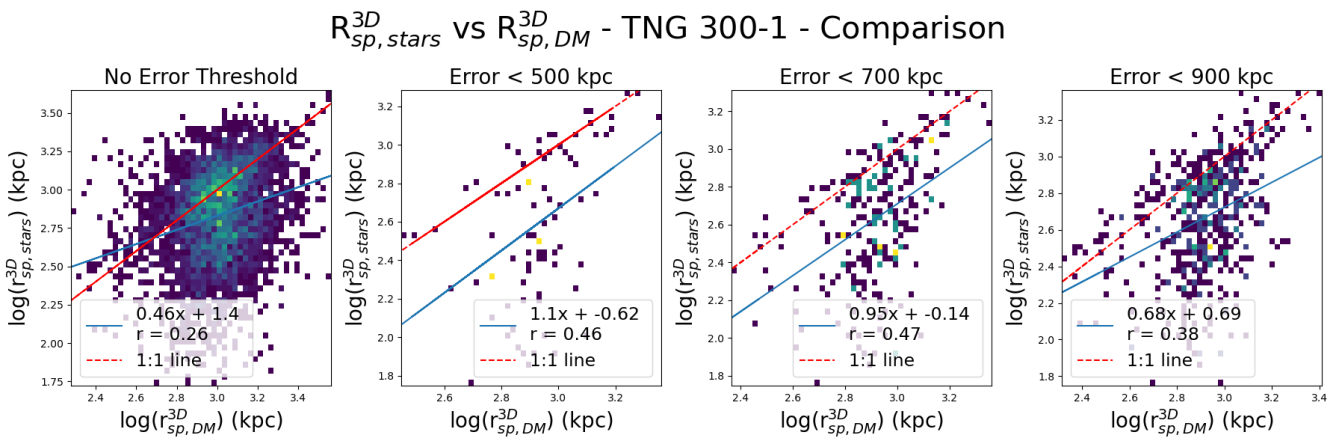

Figure 3: Comparison of the 3D derived R_{sp} with stars vs DM in TNG300-1, with an increasing constraint on the error allowed. Shown in blue is the line of best fit for the data, with the correlation written below as r. In red is a slope of 1:1. The lowest error threshold at <500kpc returns a slope of 1.1, and a correlation of r = 0.46. While this correlation is poor, we find that our Golden Sample returns the expected 1:1 slope. This spread can likely be still be decreased with higher resolution.

Figure 3). This 1:1 relation begins to diminish as our error threshold gets larger, as we can see in the far right panel. We find an interesting result that at a low error threshold, the line of best fit appears slightly vertically offset from the 1:1 relation, as the spread appears to only appear below the expected 1:1 slope in red. This could again be as a result of not removing galactic light from our stellar splashback calculation in order to retrieve ICL, a piece of the dataset we plan to fix in the future. However, the 1:1 slope that we find using calculations with low error is promising for confirming the relationship we expect.

4.1.2. *Stars vs DM in 2D*

We perform the same analysis for the correlation between calculations using stars and DM in 2D, shown in Figure 2b. In analyzing Figure 2b, we find a weak correlation for all three resolutions, with little to no change as we reduce our error threshold. There is no one resolution for which correlation is notably greater than the others; the strength of the correlation between stellar and DM splashback radii calculated in 2D seems to be independent of the resolution. There is also no error threshold for which we retrieve a greater correlation. Therefore, reducing our error threshold to attempt to constrain better results will not help our data when comparing R_{sp} results in 2D. As such, we do not create a Golden Sample in 2D for comparing stars to DM calculations, and simply compare the full dataset for each resolution.

The poor correlation in these results is likely a result of how we are calculating our 2D projection. Our small slice within the cluster is a small representation of the full cluster data, and we therefore we get a more random sampling of data. Nevertheless, this result gives us an interesting place to begin our 2D analysis as we can begin to see how calculations of a projection of a cluster compare to each other. However, we caution against a rigorous interpretation of these results, as it is not data that is representative of the full cluster. In future work, we hope to be able to better evaluate the relationship between stellar and DM calculations of R_{sp} in 2D by expanding our 2D projections to include the total cluster's data.

4.1.3. *3D vs 2D Comparison of DM*

We proceed with some caution moving forward in comparing our 2D results after seeing our comparison of stars to dark matter in 2D. However, it is still useful to attempt to interpret the results that map the same particle type in both 2D and 3D.

Naïvely, we should expect our calculations in 2D with one particle type to track reasonably well to the calculations done with the same density structure in 3D. However, outliers in our comparison of the two are reasonable to expect. Deviations are a consequence of occasionally choosing a bad angle of observation for our 2D calculations that does not accurately sample the cluster. Deviations can also occur if we retrieve a poor selection of particles due to a potentially biased sampling when drawing our cylindrical slice. Nevertheless, we should expect a relatively high correlation across dimensionality. We expect a high correlation because of how we expect clusters to function: assuming clusters are a roughly spherical structure, a 3D evaluation and a 2D slice of the same spherical density structure should return a similar radius.

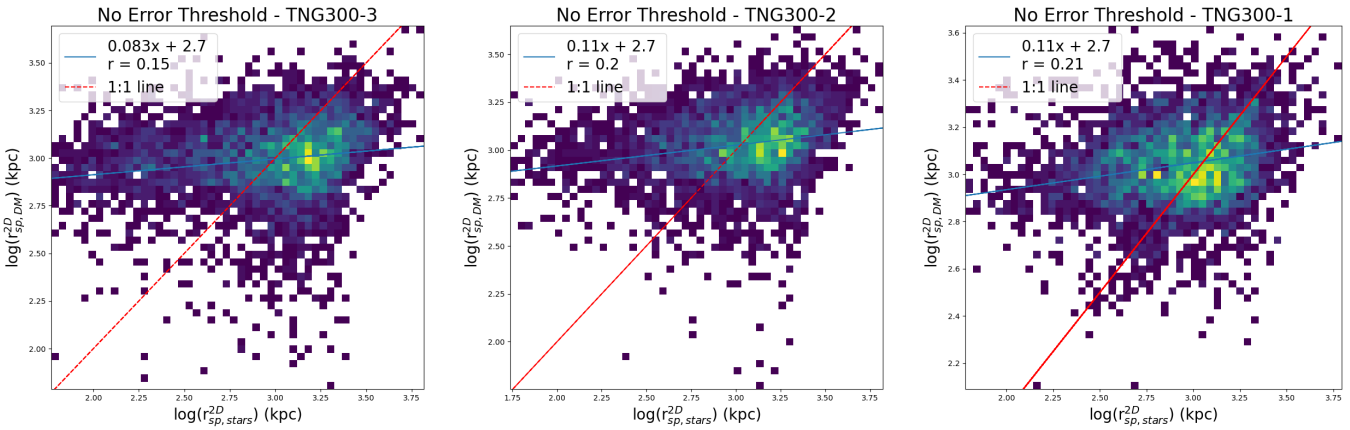

(a) Stars vs DM in 2D in TNG300-3. (b) Stars vs DM in 2D in TNG300-2. (c) Stars vs DM in 2D in TNG300-1.

Figure 4: Plots of $R^{2D}_{sp,DM}$ vs $R^{2D}_{sp,stars}$, without an error constraint. The blue line shows the line of best fit and intercept, and below is the correlation coefficient r. In red is plotted a 1:1 slope for comparison. We find a weak correlation between the two variables at each resolution.

In looking at Figure 2c, as expected, we find a high correlation between the results in 3D and 2D when comparing $R_{sp,\mathrm{DM}}$ at a low error threshold. Interestingly, we find that TNG300-1 gives us the lowest correlation between the two variables. This may imply that at higher resolution, halos are not as spherical of structures, which is an interesting result. Whereas in Figure 4 we do not need to investigate the error constraint on R_{sp}, it is wise to investigate how changing error impacts our plots of $R_{sp,\mathrm{DM}}$ in comparing 2D to 3D calculations because of how drastically the correlation changes as we change our error constraint.

In Figure 5, we find that constraining error in all 3 resolutions of TNG300 result in a tight fit around a near 1:1 correlation, as we expect. On the left, we see the entire dataset with no error threshold, and retrieve low correlations. When we restrict our errorbars to <500kpc, we find a very strong correlation of 0.91 for TNG300-3 and 300-2, and retrieve a slope of ∼0.9, demonstrating a near 1:1 relationship between the calculations. We retrieve somewhat worse results for our highest resolution, TNG300-1, with a peak correlation of only r=0.67 and a slope of 0.72. This is an interesting result, as we would hope that with an increasing resolution that our correlation would become stronger. It is possible that at the lower resolution, our halos are falsely smoother than at the highest resolution, resulting in a more spherical shape. We would hope that our highest resolution halos would be the most spherically symmetric, as this would follow the assumptions we have made up until this point, but this may be evidence for the contrary.

We find that providing a constraint on our error is critical both for removing spread around our line of best fit and retrieving a line of best fit that is closer to the 1:1 relationship that we may expect. It is unlikely that there will always be a perfect 1:1 relationship between R^{2D}_{sp} and R^{3D}_{sp} due to our angle of observation. While we assume roughly spherical shapes, many clusters are non-symmetric, and thus our calculation of R^{2D}_{sp} depends on our line of sight. As a result, it is important to understand the impact of our line of sight on the calculation of R^{2D}_{sp}, which lies in future work.

4.1.4. *3D vs 2D Comparison of Stars*

Finally, we investigate the comparison of the stellar splashback radius between 2D and 3D calculations. We find a weak correlation, only increasing slightly as we decrease our error threshold. It also does not seem to depend heavily on the simulation resolution. This is yet another intriguing result - one might expect the mapping of $R_{sp,\mathrm{stars}}$ from 2D to 3D to act much like the mapping from 2D to 3D from the DM calculation. Instead, our correlation at its greatest is only about half what it is for DM. This could be due to a difference in the distribution of stellar light throughout the cluster. We consider that DM is likely fairly smoothly distributed throughout our 2D slice, but because we are still including galactic light in our stellar calculations, we have numerous overly dense points of stellar light randomly distributed throughout our slice that are likely throwing off our calculation of R_{sp}. This provides yet more reason to proceed with ICL in the future, which may be distributed more smoothly throughout the slice.

Furthermore, the shapes of the plots comparing stars in Figure 2d are different between than in Figure 2c, where we compare DM. We find the correlation within

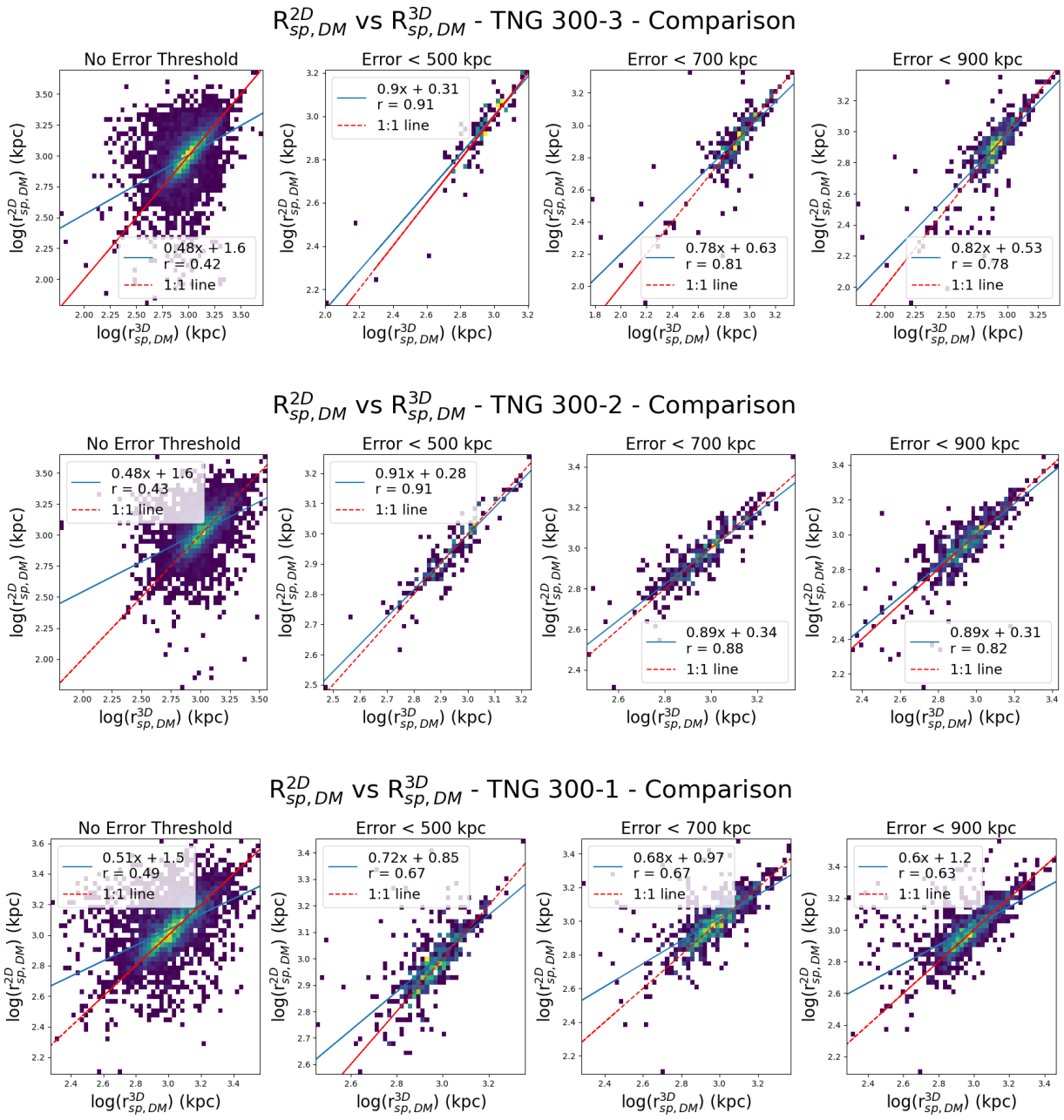

Figure 5: Comparison of 3D vs 2D R_{sp} as calculated using DM in each of the TNG300 resolutions, with an increasing constraint on the error allowed. In blue is the derived line of best fit, and in red is a 1:1 line for comparison. The correlation is given as r in the legend. We find in constraining error, we get a very near 1:1 relationship with a high correlation.

our DM plot drops off at low error thresholds, whereas for the stellar calculation it continues to rise until we reach our inner limit. However, even at its maximum, found in TNG300-2, the correlation is still mediocre, only reaching a maximum of $r \sim 0.6$. While TNG300-2 peaks very slightly higher than TNG300-1, because the three resolutions act so similarly, we choose to only investigate TNG300-1. All three resolutions follow a similar change in correlation as a function of error threshold, so we choose to only evaluate the results at one resolution. We only evaluate TNG300-1 because it should model the physics slightly more accurately, and as we have discussed in Section 4.1.1, we see a marked increase in using a higher resolution with other comparisons.

We find in Figure 6 that at low error thresholds, our correlation is strongest, but we do not find a near 1:1 relationship. Interestingly, one can pick out a number of points following the expected 1:1 relationship plotted in red, and yet even with a heavily constrained dataset we still find a wide spread outside the 1:1 line. This same trend is visible in the unconstrained dataset on the far left of Figure 6, a result that is also notable in Figure 5. This is likely again a result of our limited data in our 2D catalog along with not yet accounting for only ICL, which will be expanded upon in further work.

The comparison of the stellar splashback radius from 2D to 3D calculations demonstrates that for the time being, our 2D stellar data is least trustworthy. We have confirmed a near 1:1 relationship from Deason et al. (2020) in comparing our 3D calculations of DM and stellar splashback, demonstrating that our 3D stellar data is likely trustworthy. While we have reason to doubt our 2D data, we find a fairly strong correlation between our 2D and 3D splashback results with dark matter. The strong correlation makes some sense, as our 2D and 3D calculation from the same density fields should be similar. However, the evidence for a lack of correlation between 2D and 3D stellar splashback calculations suggests that this is where much of our error lies. This will be updated moving forward with this project.

4.2. *Future Work*

Our next steps for this project include strengthening our calculation process for our 2D catalogs, along with reevaluating the scientific method behind our stellar catalog generation.

For our 2D catalog generation, we plan to extend the length of our Fibonacci cylinder from ±4kpc from the center to $\pm 4 \times R_{200}$ in order to extend the projected line of sight to include the whole cluster. This will allow for a more holistic understanding of the particles contained within our 2D perspective of the cluster, as we would see observationally. Currently, our method only represents a small portion of what would be observed. A true 2D observation would gather light throughout the entire cluster, running from the front to the back. Our current method only accounts for a small slice in the middle of the cluster, which does not represent the rest of the matter both in front and behind the slice. Therefore, while our 3D calculations represent the total mass within the cluster, our 2D calculations only represent a small portion of the cluster mass. As such, it is reasonable to expect issues in comparing the two, as they do not represent the same total data.

Another way we can strengthen our 2D calculations is by changing the angle of observation. Currently, our 2D calculations also only choose one angle of observational when calculating the Fibonacci cylinder. We can improve this method by choosing numerous more angles at which to calculate R_{sp}, and calculating the spread in the value. Understanding the spread of R_{sp} in 2D would be immensely useful data to have, as it would provide a reasonable estimate of error on observational data. Once we have this error, we can use it to understand the correlation between our results, as demonstrated in Section 3.1, providing a reasonable understanding of how well our observations can track the underlying cluster data.

We also plan to remove the galactic stellar light from our calculations of stellar splashback. This process would involve removing stellar particles within 2× of each subhalo's stellar half mass radius and creating a new density function using the leftover stellar mass. This will provide a more accurate representation of the physical data that will be gathered, and can help better trace the underlying dark matter halo as shown in Montes & Trujillo (2018). In doing so, we hope to increase correlation between our dark matter and stellar calculations, further demonstrating that one can use the ICL to track the cluster halo.

In Section 4.1.3, we found possible evidence that at high resolution, our DM halos may begin to stray from the spherical symmetry that we have assumed up until this point. This will be an important result to clarify in the future as we regenerate our catalogs, as this is a fundamental assumption that we use throughout our calculations. As we regenerate our catalogs, we will revisit the correlation as a function of resolution to see if this relationship remains true.

These steps will allow us to better investigate how well our calculations of R_{sp} track the true data of the cluster. If we understand how a full 2D projection of the cluster instead of a small slice maps to the 3D data, we gain a powerful tool in comparing observations to the underlying cluster. Similarly, as it is understood

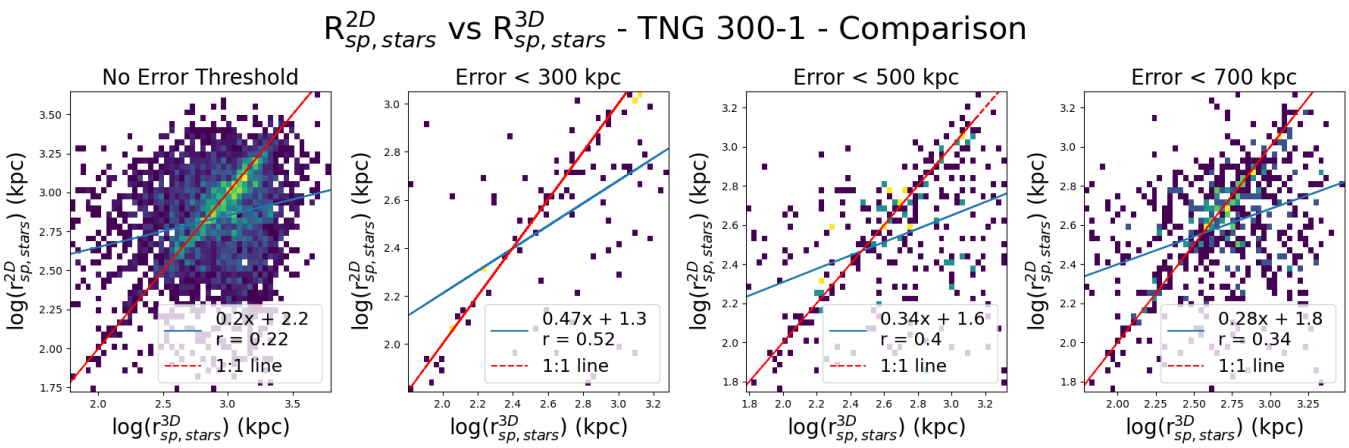

Figure 6: Comparison of the 3D derived R_{sp} with stars vs DM in TNG300-1, with an increasing constraint on the error allowed. In blue is shown the line of best fit for the data, with the correlation written below as r. In red is a slope of 1:1. The lowest error threshold at <500kpc returns a slope of 1.1, and a correlation of r = 0.46. While this correlation is poor, we find that our Golden Sample returns the expected 1:1 slope. This spread can likely be still be decreased with higher resolution.

that ICL tracks the DM halo better than total stellar light, it is important to calculate R_{sp} with ICL to better model this. Finally, understanding typical error on our calculations through changing the angle of observation is important to give us perspective on how reasonable our estimates of R_{sp} are.

5. CONCLUSION

Our work has investigated the calculation of the splashback radius within the largest box of IllustrisTNG, TNG300. We have compared calculations across particle types, notably between stellar particles and dark matter particles, in order to trace the underlying dark matter halos within galaxy clusters. We have also investigated the calculation of R_{sp} in 2D and 3D within Illustris in order to determine how well observational data can track the true underlying data of the cluster. Finally, we have compared our calculations across the three resolutions of TNG300 to investigate the impact of simulation resolution on our data. We have also created a catalog of our ideal halos with the most well constrained value of R_{sp} in order to compare correlation and an ideal relationship. In our results, we compare these variables using the Golden Sample in order to define a correlation for an ideal dataset.

Our results find the following:

(i) Using a sample with low error returns a near 1:1 relationship between stellar and DM splashback radii in 3D calculation, with an increasing correlation depending on simulation resolution.

(ii) Comparing stellar and DM splashback radii in 2D is not impacted by imposing an error threshold, and returns an unsound relationship between the two.

(iii) Comparing calculations of R_{sp} between 2D and 3D for DM show good correlation, suggesting that our 2D data can provide a reasonable understanding of the underlying cluster.

(iv) Stellar splashback radii compared between 2D and 3D calculations show a weak correlation, and a relationship that does not approach the 1:1 relation, suggesting a need to improve our stellar calculation method.

First, using our Golden Sample in our 3D calculations of stellar versus dark matter splashback radii, we find a near 1:1 relationship between stellar and DM splashback radii. This 1:1 relationship confirms findings in the literature that stellar light traces the underlying dark matter halo to a very precise level. While the correlation between the two calculations is weak, even at the highest resolution of TNG300, we find that the correlation increases as a function of resolution, implying that at an even higher resolution, we may get an even better confirmation of this relationship. Correlation increasing with resolution indicates that these results could be verified even more strongly with a higher resolution simulation. We will continue to evaluate this relationship in further work by removing light from galaxies, just leaving intracluster light. This will allow for a much more rigid analysis of the relationship between the two.

Conversely, in our 2D comparison of stellar versus dark matter splashback radii, we find that constraining our error threshold does not produce a higher correla-

tion between our results. We find almost no correlation between our results and a spread across our data that leaves our analysis of this relationship nearly obsolete. We believe that this is because of how we have generated our 2D and stellar catalogs, so this imperfect set is not a cause for concern, but an exciting place to investigate in further work.

Our results comparing R_{sp} for DM between 2D and 3D show a strong correlation as we expect, suggesting that while our method for generating 2D catalogs is still incomplete, it is not entirely flawed, and will likely provide significant results going forward. The incomplete method for 2D generation is similarly impacts our calculations for stellar splashback.

Contrarily, comparing R_{sp} for stellar light between 2D and 3D does not reveal a dependence on resolution, and a mediocre correlation between the two methods of calculation. We can track a curious spread of points along the 1:1 relation, but still find a wide spread even with a restrictive error threshold on R_{sp}. This seems to confirm that we have further steps to incorporate before we can begin a full analysis of $R_{sp,\mathrm{stars}}$.

These results are significant in that they will allow us to observationally define a radius for galaxy clusters purely using 2D observations of intracluster light that can then be mapped onto the true underlying structure of the cluster, which will help constrain our mass function for clusters throughout cosmological time, better constraining cosmological constants Ω_M and σ_8.

REFERENCES

Ade, P. A. R., Aghanim, N., Arnaud, M., et al. 2016, Astronomy amp; Astrophysics, 594, A13, doi: 10.1051/0004-6361/201525830

Adhikari, S., Dalal, N., & Chamberlain, R. T. 2014, Journal of Cosmology and Astroparticle Physics, 2014, 019–019, doi: 10.1088/1475-7516/2014/11/019

Bahcall, N. A., Dong, F., Hao, L., et al. 2003, The Astrophysical Journal, 599, 814–819, doi: 10.1086/379599

Barnes, D. J., Kay, S. T., Bahé, Y. M., et al. 2017, MNRAS, 471, 1088, doi: 10.1093/mnras/stx1647

Blumenthal, G. R., Faber, S. M., Primack, J. R., & Rees, M. J. 1984, Nature, 311, 517, doi: 10.1038/311517a0

Deason, A. J., Oman, K. A., Fattahi, A., et al. 2020, Monthly Notices of the Royal Astronomical Society, 500, 4181–4192, doi: 10.1093/mnras/staa3590

Genel, S., Vogelsberger, M., Springel, V., et al. 2014, Monthly Notices of the Royal Astronomical Society, 445, 175–200, doi: 10.1093/mnras/stu1654

Gregg, M. D., & West, M. J. 1998, Nature, 396, 549–552, doi: 10.1038/25078

Marinacci, F., Vogelsberger, M., Pakmor, R., et al. 2018, Monthly Notices of the Royal Astronomical Society, doi: 10.1093/mnras/sty2206

Monaghan, J. J., & Lattanzio, J. C. 1985, A&A, 149, 135

Montes, M., & Trujillo, I. 2018, Monthly Notices of the Royal Astronomical Society, 482, 2838–2851, doi: 10.1093/mnras/sty2858

More, S., Diemer, B., & Kravtsov, A. V. 2015, The Astrophysical Journal, 810, 36, doi: 10.1088/0004-637x/810/1/36

Naiman, J. P., Pillepich, A., Springel, V., et al. 2018, Monthly Notices of the Royal Astronomical Society, 477, 1206–1224, doi: 10.1093/mnras/sty618

Nelson, D., Pillepich, A., Springel, V., et al. 2017, Monthly Notices of the Royal Astronomical Society, 475, 624–647, doi: 10.1093/mnras/stx3040

Paulin-Henriksson, S., Antonuccio-Delogu, V., Haines, C. P., et al. 2007, Astronomy amp; Astrophysics, 467, 427–436, doi: 10.1051/0004-6361:20066994

Pillepich, A., Nelson, D., Hernquist, L., et al. 2017, Monthly Notices of the Royal Astronomical Society, 475, 648–675, doi: 10.1093/mnras/stx3112

Radovich, M., Puddu, E., Romano, A., Grado, A., & Getman, F. 2008, Astronomy amp; Astrophysics, 487, 55–61, doi: 10.1051/0004-6361:200809731

Rudick, C. S., Mihos, J. C., & McBride, C. 2006, The Astrophysical Journal, 648, 936, doi: 10.1086/506176

Sijacki, D., Vogelsberger, M., Genel, S., et al. 2015, Monthly Notices of the Royal Astronomical Society, 452, 575–596, doi: 10.1093/mnras/stv1340

Springel, V., Pakmor, R., Pillepich, A., et al. 2017, Monthly Notices of the Royal Astronomical Society, 475, 676–698, doi: 10.1093/mnras/stx3304

Vogelsberger, M., Genel, S., Springel, V., et al. 2014, Nature, 509, 177–182, doi: 10.1038/nature13316

Weinberger, R., Springel, V., Hernquist, L., et al. 2016, Monthly Notices of the Royal Astronomical Society, 465, 3291–3308, doi: 10.1093/mnras/stw2944

White, S. D. M., & Rees, M. J. 1978, Monthly Notices of the Royal Astronomical Society, 183, 341, doi: 10.1093/mnras/183.3.341